Volume 15
Number 2
14 January 2024
Pages 401–782

Chemical Science

rsc.li/chemical-science

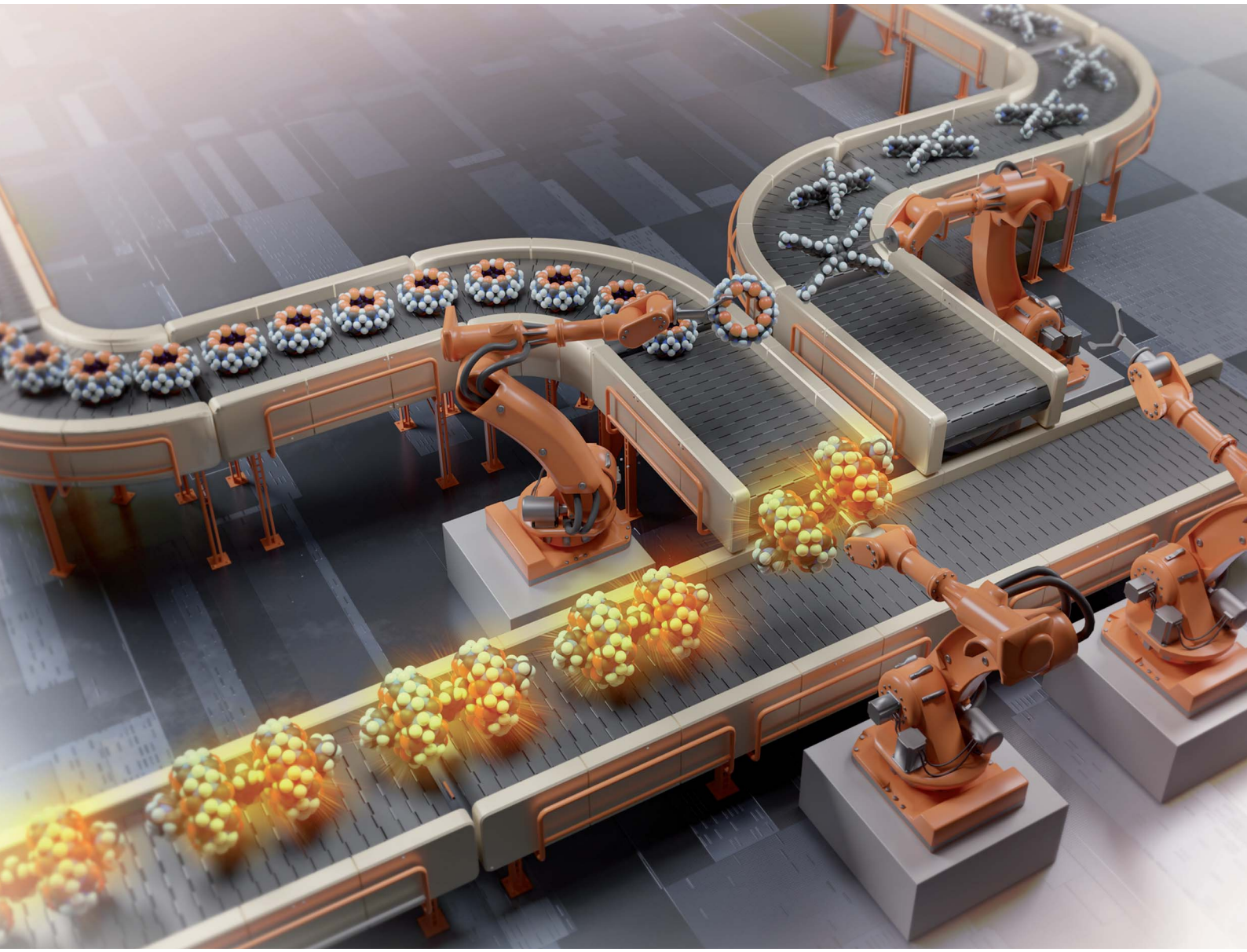

ISSN 2041-6539

ROYAL SOCIETY OF CHEMISTRY

EDGE ARTICLE

Hui Liu, Yuancheng Wang, Yingjie Zhao *et al.*
Cucurbituril-based supramolecular host–guest complexes: single-crystal structures and dual-state fluorescence enhancement

Chemical Science

ROYAL SOCIETY OF CHEMISTRY

EDGE ARTICLE

View Article Online
View Journal | View Issue

Cite this: *Chem. Sci.*, 2024, **15**, 458

All publication charges for this article have been paid for by the Royal Society of Chemistry

Received 12th September 2023
Accepted 29th November 2023

DOI: 10.1039/d3sc04813f

rsc.li/chemical-science

Cucurbituril-based supramolecular host–guest complexes: single-crystal structures and dual-state fluorescence enhancement†

Hui Wang,[ab] Hui Liu,*[a] Mingsen Wang,[a] Jiaheng Hou,[a] Yongjun Li,[c] Yuancheng Wang *[a] and Yingjie Zhao *[a]

Two supramolecular complexes were prepared using cucurbiturils [CBs] as mediators and a four-armed *p*-xylene derivative (**M1**) as a guest molecule. The single crystals of these two complexes were obtained and successfully analyzed by single-crystal X-ray diffraction (SCXRD). An unexpected and intriguing 1 : 2 self-assembly arrangement between **M1** and CB[8] was notably uncovered, marking its first observation. These host–guest complexes exhibit distinctive photophysical properties, especially emission behaviors. Invaluable insights can be derived from these single-crystal structures. The precious single-crystal structures provide both precise structural information regarding the supramolecular complexes and a deeper understanding of the intricate mechanisms governing their photophysical properties.

Introduction

Supramolecular assembly offers a bottom-up approach for constructing diversified nanostructures with precisely controlled arrangements and specific functionalities.[1–6] Host–guest molecular recognition in a supramolecular assembly is particularly valuable for achieving tunable photophysical properties in nanomaterials.[7–11] Host–guest complexes can stabilize the excited states of guest molecules, reducing non-radiative decay pathways and enhancing fluorescence emission.[12–17] This pivotal effect can lead to improved quantum yields and prolonged excited-state lifetimes, enabling tunability in the photophysical properties. As we know, the guest molecules might exhibit weak or no fluorescence in their isolated form due to molecular vibration or thermal motion.[18] However, when confined within a host's cavity, the non-radiative decay of excited states is restricted, resulting in enhanced fluorescence emission. This phenomenon is commonly referred to as aggregation-induced emission (AIE), presenting an intriguing avenue for modulating the photophysical characteristics of guest molecules. This modulation is achieved by manipulating the degree of aggregation through intricate host–guest interactions.[19–22] By carefully designing the host–guest system and manipulating their interactions, tunable emission wavelengths, fluorescence intensities, quantum yields, and other light-related behaviors can be achieved, thus paving the way for advanced applications in optoelectronics, sensors, imaging, and photonics.[23–27] Understanding these interactions helps in designing and engineering more efficient host molecules and optimizing guest binding for various applications.[24,28–31]

Cucurbiturils (CBs), esteemed as prominent macrocyclic host molecules, have exhibited remarkable proficiency in forming host–guest complexes, particularly within aqueous environments.[32–39] These host–guest complexes often exhibit tunable photophysical properties, as mentioned above. However, the acquisition of the precise structures (single crystals) of the supramolecular assemblies is always challenging. First, the guest molecules are usually larger or less compatible with the cucurbituril cavity. Stable complexes do not always readily form high-quality single crystals. Second, the host–guest complexation is usually governed by thermodynamic and kinetic factors. The kinetic trapping of the guest molecules within the cucurbituril cavity may lead to the formation of transient or metastable complexes that are challenging to crystallize.[40,41] Third, the extraordinarily large unit cell of the single crystal makes the structure determination very difficult.[42] Due to the intricate nature of their structures and the challenges associated with cultivating sizable, well-structured single crystals, a significant portion of cucurbituril-based host–guest structures remains unsolved. NMR spectroscopy, mass spectrometry, and computational modeling are still the main characterization methods that have to work in synergism to speculate the structure.

[a]*College of Polymer Science and Engineering, Qingdao University of Science and Technology, Qingdao 266042, China. E-mail: hliu@qust.edu.cn; wangyuancheng@qust.edu.cn; yz@qust.edu.cn*

[b]*College of Chemical Engineering, Qingdao University of Science and Technology, Qingdao 266042, China*

[c]*Beijing National Laboratory for Molecular Sciences (BNLMS), CAS. Key Laboratory of Organic Solids, Institute of Chemistry, Chinese. Academy of Sciences, Beijing 100190, P. R. China*

† Electronic supplementary information (ESI) available. CCDC 2285495–2285497. For ESI and crystallographic data in CIF or other electronic format see DOI: https://doi.org/10.1039/d3sc04813f

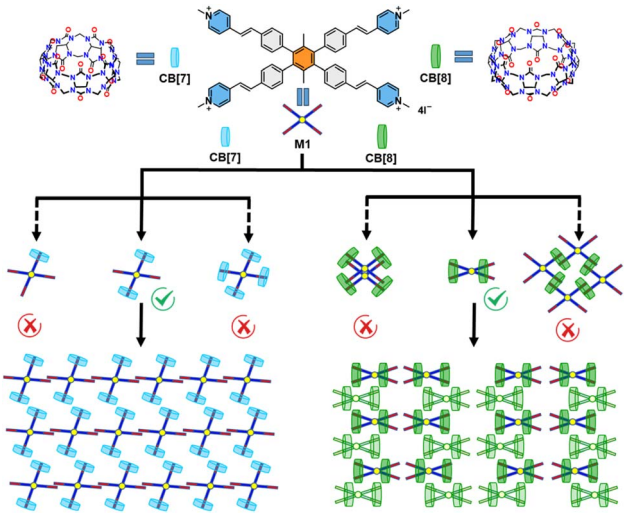

Fig. 1 The structure of **M1**, CB[7], and CB[8] and the possible self-assembly structures of **M1_CB[7]** and **M1_CB[8]**.

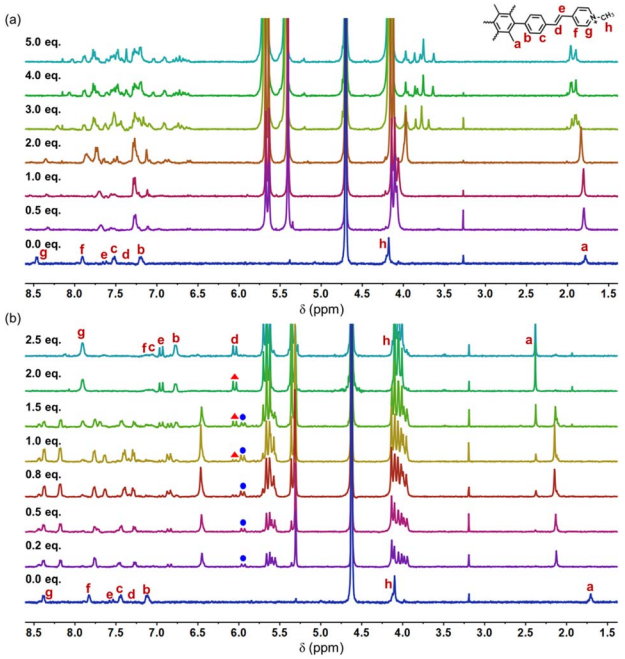

Fig. 2 ^{1}H NMR spectra of (a) **M1** (1.0 mM) in D_2O in the presence of 0, 0.5, 1.0, 2.0, 3.0, 4.0, and 5.0 equiv. of CB[7] at 25 °C; (b) **M1** (1.0 mM) in D_2O in the presence of 0, 0.2, 0.5, 0.8, 1.0, 1.5, 2.0, and 2.5 equiv. of CB[8] at 25 °C.

The precise structures of the host–guest complexes provide valuable insights into the specific non-covalent interactions between the host and guest molecules, which play a crucial role in stabilizing the complexes and realizing the tunable photophysical properties.[1,13,43–45] Herein, we designed a water-soluble four-armed guest molecule that contains hydrophobic *p*-xylene as the core and four hydrophilic styryl pyridiniums as arms. The positively charged pyridinium sites have the capacity to encapsulate within the cavities of CB[7] or CB[8], forming host–guest complexes within aqueous solutions (Fig. 1). The single-crystal X-ray diffraction (SCXRD) provided unambiguous evidence for the structures. Notably, both the **M1_CB[7]** or **M1_CB[8]** adopt a 1 : 2 self-assembly mode which is very different from the rational speculation. Unusual self-assembly behaviors were observed, especially for the **M1_CB[8]**. Two CB[8] molecules encapsulate the four arms of one **M1** molecule and form a 1 : 2 **M1_CB[8]** complex. It would be very difficult to determine the structure without the help of SCXRD. Based on the configurations of these two complexes, a modulable enhancement in fluorescence was achieved. The current design strategy, coupled with the exceptional photophysical properties arising from this intricate host–guest interaction, is anticipated to significantly broaden the range of applications for cucurbiturils in functional materials.

Results and discussion

The detailed synthesis of **M1** is presented in the ESI (Scheme S1).† The investigation into the formation of the **M1_CB[7]** and **M1_CB[8]** complexes in aqueous solution was performed through ^{1}H NMR titration. The ^{1}H NMR spectra depicting the complexes at varying **M1** to CB ratios are presented in Fig. 2. For both CB[7] and CB[8], upon introducing CBs as guest molecules, a progressive vanishing of the original monomer **M1** signals was observed, accompanied by the emergence of new H signals. These newly appearing signals were attributed to the arms encapsulated within the CBs. The observed upfield shifts of the H signals were attributed to the shielding effect exerted by the CBs. For the complex of **M1_CB[7]**, the newly appeared signals were indistinguishable and demanding to be assigned (Fig. 2a). While for **M1_CB[8]**, clear and assignable signals were observed. As shown in Fig. 2b, with the increase in CB[8], one intermediate state was clearly observed. The emergence and disappearance of the doublet peaks from the vinyl bonds solidly demonstrated this speculation. The first set of emerging signals appeared initially (marked with a blue circle). The 1.0 equiv. of CB[8] is a turning point. After this, the newly appeared first set of signals starts to disappear, with a new appearance of the second set of signals (marked with a red triangle). The addition of 1.5 equiv. of CB[8] results in the coexistence of multiple sets of new peaks, which implies multiple intermediate states during the titration process. Upon achieving a ratio of 1 : 2, the initial set of signals disappeared completely. In contrast, the freshly emerged secondary peaks exhibited a tendency towards sustained stability. Furthermore, an abundance of CB[8] failed to induce substantial alterations in the ^{1}H NMR spectra. The final state is formed with clear and assignable signals. Unlike the case of CB[7], we can clearly observe the proton signals of g, f, and c split into two sets of evenly matched peaks at the addition point of 1.0 equiv. CB[8], which indicates the formation of a relatively symmetrical structure (Fig. 2b). We speculate that this intermediate should be the species with one CB[8] over two arms in **M1** but not a structure with one CB[8] over just one arm like the CB[7] case. The findings from ^{1}H NMR titration reveal the establishment of contrasting self-assembly structures for **M1_CB[7]** and **M1_CB[8]**. Variable temperature ^{1}H NMR

experiments were then performed for **M1_CB[8]** (1 : 2) in D_2O to study the thermal stability of the complex. As shown in Fig. S6,† the split of the proton signals became better and sharper with the increase in temperatures. However, no change was observed for chemical shifts. These results indicated that the **M1_CB[8]** complexes were still stable at 90 °C and did not undergo the process of dissociation.

Macrocyclic host molecules, referred to as CBs, exhibit a distinctive arrangement featuring a hydrophobic cavity and a periphery abundant in carbonyl groups. This structural design, tailored to cavity dimensions, endows CBs with notably high binding constants when engaging a diverse range of guests within aqueous solutions. This exceptional affinity underscores their exceptional capability to provide robust protection for entrapped guests. The small cavity of CB[7] typically accommodates a single guest molecule.[14] In contrast, CB[8], possessing a larger cavity, exhibits the unique capability of simultaneously binding two guest molecules.[1,14,46–48] Thus, based on the conventional experience and analysis of ^{1}H NMR titration data, several possible self-assembly structures can be proposed. As shown in Fig. 1, possible structures of **M1_CB[7]** could be 1 : 1, 1 : 2, or 1 : 4 complexes. More diversified structures can be predicted for **M1_CB[8]**. For example, a dimer has been observed by our group in a previous study.[14] A two-dimensional (2D) extended network has also been proposed by other research groups and us.[6,49–52] However, it will be difficult to elucidate the precise structure without the evidence of crystallographic data.

To unveil precise structural insights into the host–guest supramolecular complexes of **M1_CB[7]** and **M1_CB[8]**, we employed the highly effective technique of SCXRD. Fortunately, both the **M1_CB[7]** and **M1_CB[8]** supramolecular complexes yielded single crystals through gradual cooling of nearly saturated aqueous solutions. The detailed preparation of the single crystals of **M1_CB[7]** and **M1_CB[8]** is presented in the ESI.† **M1_CB[7]** exhibits prismatic shapes from the optical microscopy images (Fig. 3a). The morphological characteristics of the self-assembled structures formed by **M1** and CB[8] were subsequently subjected to comprehensive analysis. Optical microscopy, atomic force microscopy (AFM), scanning electron microscopy (SEM), and transmission electron microscopy (TEM) investigations collectively unveiled the emergence of orderly square structures (Fig. 3b–f). These square structures exhibit an average side length spanning 100–300 mm. Remarkably, AFM cross-section analyses disclosed a layer-by-layer arrangement (Fig. 3e and f), with each layer measuring approximately 1.9 nm in thickness, consistent with the outer diameter of CB[8] at 1.75 nm (Fig. 3f). In tandem with the insights garnered from ^{1}H NMR titration, these findings strongly indicate that the self-assembly process of **M1** and CB[8] potentially gives rise to a 2D supramolecular complex, as shown in the proposed structure in Fig. 1. To validate this speculation, the acquirement of the single crystal structure is necessary.

Crystallographic data detailing the supramolecular complexes are accessible through the Cambridge Crystallographic Data Center, specifically identified as CCDC 2285496 (**M1_CB[7]**) and CCDC 2285497 (**M1_CB[8]**). Notably, the single crystal structure of **M1_CB[7]** conforms to the $P\bar{1}$ space group, characterized by distinct cell parameters: a = 13.1070 Å, b = 17.0258 Å, c = 25.9476 Å, α = 75.072°, β = 85.004°, and γ = 77.546°. This structural arrangement, influenced by the confined cavity of CB[7], permits the accommodation of solely one vinyl pyridinium arm from the guest molecule. This is consistent with our speculation. Notably, a 1 : 2 **M1_CB[7]** complex was realized according to the single crystal structure analysis (Fig. 4). Two CB[7] molecules encapsulated two ortho arms of one **M1** molecule (Fig. 4a and b). The two left unencapsulated ortho arms are aligned in parallel to form a linear self-assembly structure. The linear self-assemblies were then aligned in parallel to form the final packing structure (Fig. 4b and c). The distance between the end of the two arms in the **M1** molecule is around 14.9 Å (Fig. 4a). And the distance between the unencapsulated arms is around 4.9 Å (Fig. 4b).

In the case of **M1_CB[8]**, the individual crystal structure conforms to the $P\bar{4}2c$ space group, featuring specific cell parameters: a = 18.6227 Å, b = 18.6227 Å, c = 90.614 Å, α = 90°, β = 90°, and γ = 90°. As shown in Fig. 5, rather than giving rise to a 2D supramolecular arrangement, a distinctive 1 : 2 **M1_CB[8]** complex materializes, wherein two CB[8] molecules encapsulate the four arms of one **M1** molecule. Each CB[8] molecule adeptly encapsulates the two neighboring arms of **M1**. This specific configuration, hitherto unprecedented in CB-based host–guest complexes, engenders a high degree of interest. Encouragingly, these findings are also highly consistent with the outcomes derived from the ^{1}H NMR titration experiments. The distance between the two arms of one **M1** molecule marvelously decreased to 3.9 Å (Fig. 5a). A completely unexpected structure with a single **M1** molecule was formed. In addition, the positions of the two CB[8] molecules in **M1** are asymmetrical. One of the CB[8] molecules is next to the benzene core, and the other one is located at the end of the arms. The individual 1 : 2 **M1_CB[8]** complex then adopts an alternated arrangement along the a and c axes to finally realize the crystal packing. The space between the individual **M1_CB[8]** complex is

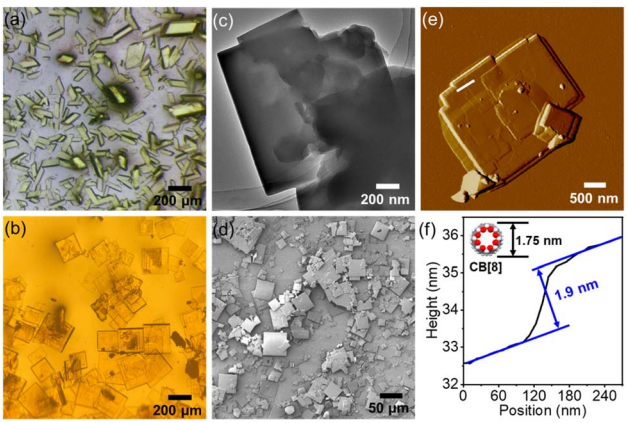

Fig. 3 (a) Optical microscope image of **M1_CB[7]** crystals. (b) Optical microscope image of **M1_CB[8]** crystals. (c) TEM image of **M1_CB[8]**. (d) SEM image of **M1_CB[8]**. (e) AFM image of **M1_CB[8]**. (f) The height analysis of **M1_CB[8]** from the AFM image.

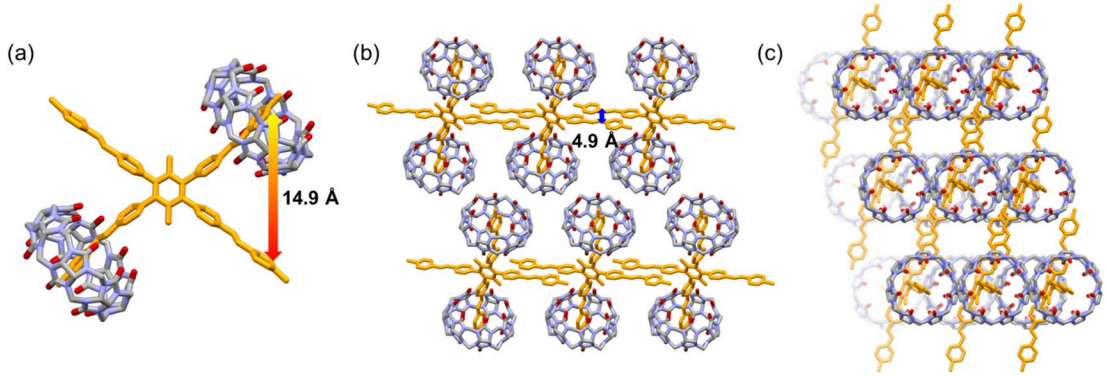

Fig. 4 X-ray crystal structures of **M1_CB[7]**. (a) Crystal structure of the 1 : 2 **M1_CB[7]** host–guest complex. (b) Side view of the packing mode. (c) Top view of the packing mode.

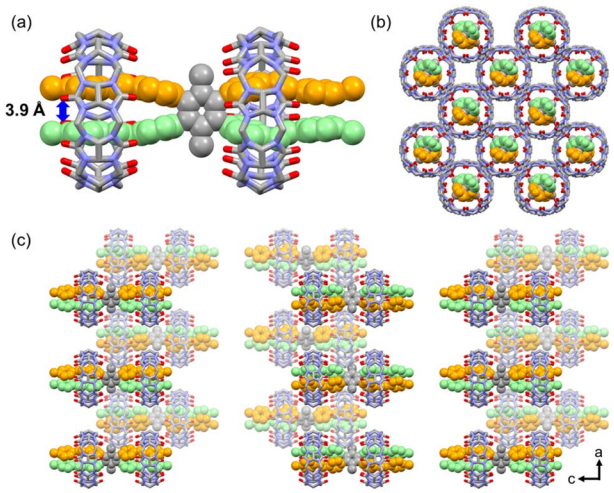

Fig. 5 X-ray crystal structure of **M1_CB[8]**. (a) Crystal structure of the 1 : 2 **M1_CB[8]** host–guest complex. (b) Top view of the packing mode. (c) Side view of the packing mode.

filled with disordered solvent and CB[8] molecules. For clarity reasons, these molecules were omitted in the images.

As shown in Fig. 6, significant color and fluorescence changes were observed by the naked eye for both the solutions and single crystals of **M1_CB[7]** and **M1_CB[8]** complexes compared to monomeric **M1**. The solution of **M1_CB[7]** does not exhibit an obvious color change compared to **M1** under visible light, while **M1_CB[8]** solution became obviously yellow (Fig. 6a). A more interesting phenomenon was observed in the fluorescence of **M1_CB[7]** and **M1_CB[8]**. As shown in Fig. 6b, under the irradiation of a UV lamp at 365 nm, it could be clearly observed that the fluorescence of **M1**, **M1_CB[7]**, and **M1_CB[8]** solutions was enhanced gradually. The **M1_CB[8]** solution showed bright orange fluorescence. Moreover, the solid state of **M1_CB[8]** exhibits similar fluorescence behavior to its solution state. Obvious bright orange fluorescence was observed for the **M1_CB[8]** crystal (Fig. 6h). In contrast, the fluorescence of **M1** and **M1_CB[7]** crystals under UV lamp irradiation at 365 nm is not as obvious as that of their solution state (Fig. 6c–h). The obvious changes in the colors and the fluorescence from **M1** to the complexes of **M1_CB[7]** and **M1_CB[8]**, which can be observed by the naked eye, originate from their distinct electronic structures. Notably, **M1_CB[8]** exhibits strong fluorescence both in solutions and solid states, which has been affirmed as dual-state emission (DSE).[53–55] Fortunately, the single crystal structures of **M1_CB[7]** and **M1_CB[8]** are available to help us to reveal the mechanism of the variation in photophysical properties. The intricate process of complex formation between CBs and **M1** exerts an influence on the coupling degree and hybrid band structure of the **M1** molecule, thereby resulting in profound changes in photophysical attributes. These changes encompass parameters like the emission wavelength and fluorescence quantum yield, resulting in profound modifications.[56,57] Thus, the photophysical properties of **M1**, **M1_CB[7]**, and **M1_CB[8]** were further studied. According to the precious complex structures from the single crystal analysis, the structure–property relationship can be accurately explored.

As shown in Fig. 7a, **M1** displayed a prominent absorption peak at 356 nm and a fluorescence peak at 537 nm. Upon the introduction of CB[7], the UV-vis absorption peak red-shifted

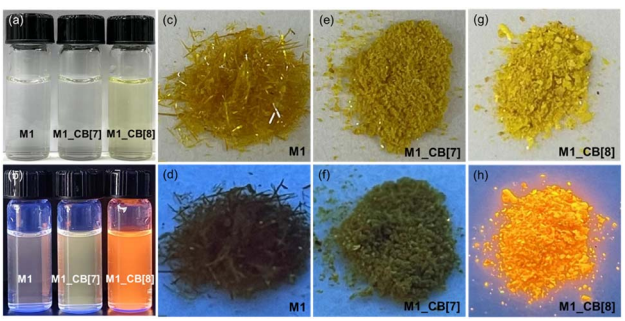

Fig. 6 (a) The photographs of **M1**, **M1_CB[7]** and **M1_CB[8]** solution (10^{-5} M in H_2O) in visible light. (b) The luminescence photographs of **M1**, **M1_CB[7]** and **M1_CB[8]** solution (10^{-5} M in H_2O) under 365 nm UV light. The photographs of **M1** (c), **M1_CB[7]** (e) and **M1_CB[8]** (g) crystals in visible light. The luminescence photographs of **M1** (d), **M1_CB[7]** (f) and **M1_CB[8]** (h) crystals under 365 nm UV light.

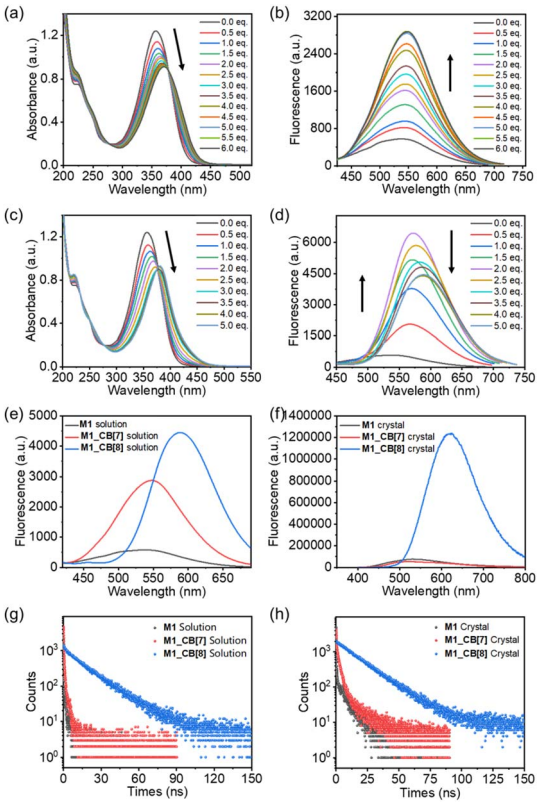

Fig. 7 (a) UV-vis and (b) fluorescence spectra titrations of **M1** (10^{-5} M) upon addition of CB[7] in water; (c) UV-vis and (d) fluorescence spectra titrations of **M1** (10^{-5} M) upon addition of CB[8] in water. Fluorescence spectra of **M1**, **M1_CB[7]**, and **M1_CB[8]** solutions (10^{-5} M) (e) and crystals (f). Time-resolved decay spectra of **M1**, **M1_CB[7]**, and **M1_CB[8]** solutions (g) and crystals (h) (λ_{ex} = 375 nm).

from 356 nm to 370 nm (Δ = 14 nm) with a 25% decrease in intensity. Concurrently, the fluorescence emission peak shifted from 537 nm to 547 nm (Δ = 10 nm), showcasing a noteworthy fivefold enhancement in fluorescence intensity (Fig. 7b). In the case of **M1_CB[8]**, the UV-vis absorption peak experienced a red shift from 356 nm to 380 nm (Δ = 24 nm) with a 24% decrease in intensity (Fig. 7c). Additionally, the fluorescence emission peak shifted from 537 nm to 589 nm (Δ = 52 nm), resulting in a remarkable nine-fold enhancement in fluorescence intensity (Fig. 7d). Notably, unlike CB[7], the addition of CB[8] generated an intermediate state according to the fluorescence titration of **M1** with CB[8]. From the addition of 0.5 to 2.0 equiv. CB[8], no obvious redshift occurred. Only increased intensity was observed. The strongest fluorescence emission was realized when the addition of CB[8] reached ~2.0 equiv. Afterward, the fluorescence intensity starts to decrease with an obvious red shift gradually. When introducing four equiv. CB[8], the titration reaches its endpoint (Fig. 7d). This observation is highly consistent with the ^{1}H NMR titration results. However, the amounts of CB[8] required to reach the endpoint in the ^{1}H NMR (~2.0 equiv) and fluorescence (~4.0 equiv) titration are different. This is due to the concentration difference, which may induce different dynamic equilibrium processes during the self-assembly. Notably, a tendency of a gradual increase in the fluorescence intensity was observed for the solution of **M1**, **M1_CB[7]**, and **M1_CB[8]** (Fig. 7e). In contrast, the solid-state fluorescence of **M1**, **M1_CB[7]**, and **M1_CB[8]** exhibits different behaviors. The **M1_CB[7]** single crystal does not exhibit an obvious increase compared to **M1**, while a sharp increase for the **M1_CB[8]** single crystal is observed (Fig. 7f). The AIE phenomenon was only observed for **M1_CB[8]**, which also exhibits strong solution state fluorescence. The quantum yields of **M1_CB[7]** and **M1_CB[8]** in water were measured to be 3.03% and 24.40%, which are 5 times and 46 times larger than the 0.52% quantum yield of **M1** itself in aqueous solution (Table 1). In the solid state, the fluorescence quantum yields of **M1**, **M1_CB[7]**, and **M1_CB[8]** single crystals were measured to be 0.02%, 1.27%, and 22.32% (Table 1), which is consistent with the fluorescence spectra (Fig. 7e and f). The emission lifetimes of **M1_CB[7]** and **M1_CB[8]** were measured to be 0.54 ns, 0.89 ns, and 16.80 ns in aqueous solution (Fig. 7g and Table 1) and 3.78 ns, 4.60 ns, and 17.04 ns in the solid state (Fig. 7h and Table 1).

As described above, **M1_CB[8]** exhibited more pronounced alterations in UV-vis and fluorescence spectra when contrasted with **M1_CB[7]**. This phenomenon is intimately linked to the intricate complexation structures of **M1_CB[7]** and **M1_CB[8]**. According to the SCXRD data, CB[7] and CB[8] form 2 : 1 complexes with the **M1** molecule, respectively. In the **M1_CB[7]** complex, only two arms of the **M1** molecule are encapsulated within the cavity of CB[7], while the remaining two arms are still in a free state. However, in the **M1_CB[8]** complex, all four arms of the **M1** molecule are fully encapsulated within the cavity of CB[8], effectively constraining the vibrational motion of **M1**, which in turn suppresses the non-radiative decay of **M1** and enhances its fluorescence intensity.[1,58–61] The evidence for this conclusion is also supported by the higher ratio of radiative (k_r) and nonradiative (k_{nr}) decay rates in aqueous solutions, which have been measured to be 5.3×10^{-3} (**M1**), 3.1×10^{-2} (**M1_CB[7]**), and 3.4×10^{-1} (**M1_CB[8]**). The ratios in the solid state were measured to be 2.1×10^{-4} (**M1**), 1.3×10^{-2} (**M1_CB[7]**), and 2.8×10^{-1} (**M1_CB[8]**), which is consistent with the values in the solution state (Table 1).[62]

Therefore, we hypothesize that this fluorescence enhancement phenomenon arises from the unique supramolecular aggregation effect mediated by CBs. The encapsulation of the **M1** within the CB[8] cavity greatly stabilized the excited states of **M1**, which can be clearly concluded from the evidence of the single crystal structure. This stabilization hinders the non-radiative decay pathways available to **M1** in its free state.[1] The guest molecule has to spend more time in the excited state before returning to the ground state through emission, thus leading to longer emission lifetimes.[13] The restricted motion inhibits the relaxation dynamics of **M1** and enhances the radiative decay (emission) pathway, leading to an increase in the fluorescence quantum yield in both the solution and solid state.[63]

CB[7] with a smaller cavity can partially encapsulate the **M1** molecules, which is also evidenced by the single crystal analysis. The degrees of the stabilization of the excited states and the restriction of the motion for the **M1** molecules can be finely

Table 1 Photophysical data for **M1**, **M1_CB[7]** and **M1_CB[8]** under ambient

Compounds[b]	Solvent	Ex [nm]	Em [nm]	$\tau_{avg.}$[a] [ns]	ϕ_{FL} (%)	k_r[c] [nm]	k_{nr}[d] [ns]	k_r/k_{nr}
M1 solution	H_2O	375	537	0.54	0.52	9.6×10^{-3}	1.8	5.3×10^{-3}
M1_CB[7] solution	H_2O	375	547	0.89	3.03	3.4×10^{-2}	1.1	3.1×10^{-2}
M1_CB[8] solution	H_2O	375	590	16.80	24.40	1.5×10^{-2}	4.4×10^{-2}	3.4×10^{-1}
M1 crystal	—	375	533	3.78	0.02	5.3×10^{-5}	2.6×10^{-1}	2.1×10^{-4}
M1_CB[7] crystal	—	375	520	4.60	1.27	2.8×10^{-3}	2.1×10^{-1}	1.3×10^{-2}
M1_CB[8] crystal	—	375	620	17.04	22.32	1.3×10^{-2}	4.6×10^{-2}	2.8×10^{-1}

[a] Lifetimes were measured using an EPL picosecond pulsed diode laser (375 nm) as a light source. [b] The absolute photoluminescent quantum yield of **M1**, **M1_CB[7]**, and **M1_CB[8]** under ambient (air) were measured using an integrating sphere. [c] The radiative decay rate constant of fluorescence $k_r = \phi_{FL}/\tau$. [d] The nonradiative decay rate constant of phosphorescence $k_{nr} = \tau_{avg.}^{-1} - k_r$.

tuned to realize the controllable photophysical properties. Thanks to the clear structures provided by the single crystal analysis, detailed and clear mechanisms behind the changes in photophysical properties in these supramolecular complexes are clarified.

Conclusions

In summary, two distinct self-assembled configurations involving the guest molecule **M1** and CB[7] or CB[8] in an aqueous medium were successfully realized through host–guest interactions. The unequivocal elucidation of supramolecular complex structures was facilitated by SCXRD analysis. Due to the different assembly modes of the two complexes, tunable photophysical properties are realized through the influence of non-radiative attenuation, especially for the emission behavior of the complex **M1_CB[8]**. A noticeable enhancement in the fluorescence quantum yield and prolonged emission lifetime was obtained for this very unusual self-assembled structure. This sample supramolecular self-assembly strategy offers a versatile platform to manipulate and control the photophysical properties of guest molecules and may open up new avenues for various applications, ranging from light-emitting materials to sensors and molecular devices.

Data availability

Crystallographic data for [**S5**, **M1_CB[7]**, **M1_CB[8]**] has been deposited at the [CCDC] under [2285495–2285497] and can be obtained from [**https://www.ccdc.cam.ac.uk/data_request/cif**].

Author contributions

H. Wang performed the synthesis, single crystals growth, characterization, and photophysical tests. H. Liu directed the synthesis and self-assembly part. M. Wang and J. Hou helped with the synthesis. Y. Li helped to perform the single crystal X-ray diffraction measurements. Y. Wang directed the photophysical tests part. Y. Zhao designed and supervised the project and wrote the manuscript.

Conflicts of interest

The authors declare no competing financial interest.

Acknowledgements

Acknowledgments are extended to the National Key Research and Development Program of China (2022YFB3805101), the National Natural Science Foundation of China (22205128, 22175101, and 22275107), and the Natural Science Foundation of Shandong Province (ZR2022QB054 and ZR2020ZD38) for their valuable financial support.

References

1 J. Wang, Z. Huang, X. Ma and H. Tian, Visible-Light-Excited Room-Temperature Phosphorescence in Water by Cucurbit [8]uril-Mediated Supramolecular Assembly, *Angew. Chem., Int. Ed.*, 2020, **59**, 9928–9933.
2 B. Tang, J. Zhao, J.-F. Xu and X. Zhang, Tuning the stability of organic radicals: from covalent approaches to non-covalent approaches, *Chem. Sci.*, 2020, **11**, 1192–1204.
3 D. Xia, P. Wang, X. Ji, N. M. Khashab, J. L. Sessler and F. Huang, Functional Supramolecular Polymeric Networks: The Marriage of Covalent Polymers and Macrocycle-Based Host–Guest Interactions, *Chem. Rev.*, 2020, **120**, 6070–6123.
4 W. Zhang, Y.-M. Zhang, S.-H. Li, Y.-L. Cui, J. Yu and Y. Liu, Tunable Nanosupramolecular Aggregates Mediated by Host–Guest Complexation, *Angew. Chem., Int. Ed.*, 2016, **55**, 11452–11456.
5 E. A. Appel, J. del Barrio, X. J. Loh and O. A. Scherman, Supramolecular polymeric hydrogels, *Chem. Soc. Rev.*, 2012, **41**, 6195–6214.
6 B. Yang, S.-B. Yu, P.-Q. Zhang, Z.-K. Wang, Q.-Y. Qi, X.-Q. Wang, X.-H. Xu, H.-B. Yang, Z.-Q. Wu, Y. Liu, D. Ma and Z.-T. Li, Self-Assembly of a Bilayer 2D Supramolecular Organic Framework in Water, *Angew. Chem., Int. Ed.*, 2021, **60**, 26268–26275.
7 R. N. Dsouza, U. Pischel and W. M. Nau, Fluorescent Dyes and Their Supramolecular Host/Guest Complexes with Macrocycles in Aqueous Solution, *Chem. Rev.*, 2011, **111**, 7941–7980.
8 W.-W. Xu, Y. Chen, Y.-L. Lu, Y.-X. Qin, H. Zhang, X. Xu and Y. Liu, Tunable Second-Level Room-Temperature Phosphorescence of Solid Supramolecules between Acrylamide–Phenylpyridium Copolymers and Cucurbit[7] uril, *Angew. Chem., Int. Ed.*, 2022, **61**, e202115265.

9 X.-L. Ni, S. Chen, Y. Yang and Z. Tao, Facile Cucurbit[8]uril-Based Supramolecular Approach To Fabricate Tunable Luminescent Materials in Aqueous Solution, *J. Am. Chem. Soc.*, 2016, **138**, 6177–6183.

10 M. Huo, X.-Y. Dai and Y. Liu, Uncommon Supramolecular Phosphorescence-Capturing Assembly Based on Cucurbit[8]uril-Mediated Molecular Folding for Near-Infrared Lysosome Imaging, *Small*, 2022, **18**, 2104514.

11 Y. Luo, W. Zhang, M. X. Yang, X. H. Feng, C. Redshaw, Q. Li, Z. Tao and X. Xiao, A Twisted Cucurbit[14]Uril-Based Fluorescent Supramolecular Polymer Mediated by Metal Ion, *Macromolecules*, 2022, **55**, 1642–1646.

12 H.-Y. Zhou, D.-W. Zhang, M. Li and C.-F. Chen, A Calix[3]acridan-Based Host–Guest Cocrystal Exhibiting Efficient Thermally Activated Delayed Fluorescence, *Angew. Chem., Int. Ed.*, 2022, **61**, e202117872.

13 W.-L. Zhou, Y. Chen, Q. Yu, H. Zhang, Z.-X. Liu, X.-Y. Dai, J.-J. Li and Y. Liu, Ultralong purely organic aqueous phosphorescence supramolecular polymer for targeted tumor cell imaging, *Nat. Commun.*, 2020, **11**, 4655.

14 H. Liu, M. Lin, Y. Cui, W. Gan, J. Sun, B. Li and Y. Zhao, Single-crystal structures of cucurbituril-based supramolecular host–guest complexes for bioimaging, *Chem. Commun.*, 2021, **57**, 10190–10193.

15 X.-K. Ma, W. Zhang, Z. Liu, H. Zhang, B. Zhang and Y. Liu, Supramolecular Pins with Ultralong Efficient Phosphorescence, *Adv. Mater.*, 2021, **33**, 2007476.

16 H. Nie, Z. Wei, X.-L. Ni and Y. Liu, Assembly and Applications of Macrocyclic-Confinement-Derived Supramolecular Organic Luminescent Emissions from Cucurbiturils, *Chem. Rev.*, 2022, **122**, 9032–9077.

17 T. Zhang, X. Ma, H. Wu, L. Zhu, Y. Zhao and H. Tian, Molecular Engineering for Metal-Free Amorphous Materials with Room-Temperature Phosphorescence, *Angew. Chem., Int. Ed.*, 2020, **59**, 11206–11216.

18 Y. Huang, J. Xing, Q. Gong, L.-C. Chen, G. Liu, C. Yao, Z. Wang, H.-L. Zhang, Z. Chen and Q. Zhang, Reducing aggregation caused quenching effect through co-assembly of PAH chromophores and molecular barriers, *Nat. Commun.*, 2019, **10**, 169.

19 J. Luo, Z. Xie, J. W. Y. Lam, L. Cheng, H. Chen, C. Qiu, H. S. Kwok, X. Zhan, Y. Liu, D. Zhu and B. Z. Tang, Aggregation-induced emission of 1-methyl-1,2,3,4,5-pentaphenylsilole, *Chem. Commun.*, 2001, 1740–1741.

20 Kenry, B. Z. Tang and B. Liu, Catalyst: Aggregation-Induced Emission—How Far Have We Come, and Where Are We Going Next?, *Chem*, 2020, **6**, 1195–1198.

21 J. Mei, N. L. C. Leung, R. T. K. Kwok, J. W. Y. Lam and B. Z. Tang, Aggregation-Induced Emission: Together We Shine, United We Soar, *Chem. Rev.*, 2015, **115**, 11718–11940.

22 Y. Hong, J. W. Y. Lam and B. Z. Tang, Aggregation-induced emission, *Chem. Soc. Rev.*, 2011, **40**, 5361–5388.

23 Q. Song, Y. Jiao, Z. Wang and X. Zhang, Tuning the Energy Gap by Supramolecular Approaches: Towards Near-Infrared Organic Assemblies and Materials, *Small*, 2016, **12**, 24–31.

24 M. Tian, Z. Wang, X. Yuan, H. Zhang, Z. Liu and Y. Liu, Configurationally Confined Multilevel Supramolecular Assemblies for Modulating Multicolor Luminescence, *Adv. Funct. Mater.*, 2023, **33**, 2300779.

25 H. Sun and L. Zhu, Achieving purely organic room temperature phosphorescence in aqueous solution, *Aggregate*, 2023, **4**, e253.

26 D. Li, Z. Feng, Y. Han, C. Chen, Q.-W. Zhang and Y. Tian, Time-Resolved Encryption via a Kinetics-Tunable Supramolecular Photochromic System, *Adv. Sci.*, 2022, **9**, 2104790.

27 M. Yan, S. Wu, Y. Wang, M. Liang, M. Wang, W. Hu, G. Yu, Z. Mao, F. Huang and J. Zhou, Recent Progress of Supramolecular Chemotherapy Based on Host–Guest Interactions, *Adv. Mater.*, 2023, 2304249.

28 C. Xu, C. Yin, W. Wu and X. Ma, Tunable room-temperature phosphorescence and circularly polarized luminescence encoding helical supramolecular polymer, *Sci. China: Chem.*, 2022, **65**, 75–81.

29 C. Wang, X.-K. Ma, P. Guo, C. Jiang, Y.-H. Liu, G. Liu, X. Xu and Y. Liu, Highly Reversible Supramolecular Light Switch for NIR Phosphorescence Resonance Energy Transfer, *Adv. Sci.*, 2022, **9**, 2103041.

30 X. Ma, J. Wang and H. Tian, Assembling-Induced Emission: An Efficient Approach for Amorphous Metal-Free Organic Emitting Materials with Room-Temperature Phosphorescence, *Acc. Chem. Res.*, 2019, **52**, 738–748.

31 H. Wang, X. Ji, Z. Li and F. Huang, Fluorescent Supramolecular Polymeric Materials, *Adv. Mater.*, 2017, **29**, 1606117.

32 J. Lagona, P. Mukhopadhyay, S. Chakrabarti and L. Isaacs, The Cucurbit[n]uril Family, *Angew. Chem., Int. Ed.*, 2005, **44**, 4844–4870.

33 K. I. Assaf and W. M. Nau, Cucurbiturils: from synthesis to high-affinity binding and catalysis, *Chem. Soc. Rev.*, 2015, **44**, 394–418.

34 S. J. Barrow, S. Kasera, M. J. Rowland, J. del Barrio and O. A. Scherman, Cucurbituril-Based Molecular Recognition, *Chem. Rev.*, 2015, **115**, 12320–12406.

35 J. W. Lee, S. Samal, N. Selvapalam, H.-J. Kim and K. Kim, Cucurbituril Homologues and Derivatives: New Opportunities in Supramolecular Chemistry, *Acc. Chem. Res.*, 2003, **36**, 621–630.

36 Y.-H. Liu, Y.-M. Zhang, H.-J. Yu and Y. Liu, Cucurbituril-Based Biomacromolecular Assemblies, *Angew. Chem., Int. Ed.*, 2021, **60**, 3870–3880.

37 Y. Huang, R.-H. Gao, M. Liu, L.-X. Chen, X.-L. Ni, X. Xiao, H. Cong, Q.-J. Zhu, K. Chen and Z. Tao, Cucurbit[n]uril-Based Supramolecular Frameworks Assembled through Outer-Surface Interactions, *Angew. Chem., Int. Ed.*, 2021, **60**, 15166–15191.

38 R.-H. Gao, Y. Huang, K. Chen and Z. Tao, Cucurbit[n]uril/metal ion complex-based frameworks and their potential applications, *Coord. Chem. Rev.*, 2021, **437**, 213741.

39 B. Tang, J. Zhao, J.-F. Xu and X. Zhang, Cucurbit[n]urils for Supramolecular Catalysis, *Chem. - Eur. J.*, 2020, **26**, 15446–15460.

40 C. Márquez, R. R. Hudgins and W. M. Nau, Mechanism of Host–Guest Complexation by Cucurbituril, *J. Am. Chem. Soc.*, 2004, **126**, 5806–5816.
41 O. Danylyuk, V. P. Fedin and V. Sashuk, Kinetic trapping of the host–guest association intermediate and its transformation into a thermodynamic inclusion complex, *Chem. Commun.*, 2013, **49**, 1859–1861.
42 Z. Huang, E. S. Grape, J. Li, A. K. Inge and X. Zou, 3D electron diffraction as an important technique for structure elucidation of metal-organic frameworks and covalent organic frameworks, *Coord. Chem. Rev.*, 2021, **427**, 213583.
43 W. Zhu, Y. Li, S. Guo, W.-J. Guo, T. Peng, H. Li, B. Liu, H.-Q. Peng and B. Z. Tang, Stereoisomeric engineering of aggregation-induced emission photosensitizers towards fungal killing, *Nat. Commun.*, 2022, **13**, 7046.
44 W.-L. Zhou, W. Lin, Y. Chen and Y. Liu, Supramolecular assembly confined purely organic room temperature phosphorescence and its biological imaging, *Chem. Sci.*, 2022, **13**, 7976–7989.
45 H.-J. Yu, Q. Zhou, X. Dai, F.-F. Shen, Y.-M. Zhang, X. Xu and Y. Liu, Photooxidation-Driven Purely Organic Room-Temperature Phosphorescent Lysosome-Targeted Imaging, *J. Am. Chem. Soc.*, 2021, **143**, 13887–13894.
46 J. d. Barrio, J. Liu, R. A. Brady, C. S. Y. Tan, S. Chiodini, M. Ricci, R. Fernández-Leiro, C.-J. Tsai, P. Vasileiadi, L. Di Michele, D. Lairez, C. Toprakcioglu and O. A. Scherman, Emerging Two-Dimensional Crystallization of Cucurbit[8]uril Complexes: From Supramolecular Polymers to Nanofibers, *J. Am. Chem. Soc.*, 2019, **141**, 14021–14025.
47 B. Yang, S.-B. Yu, H. Wang, D.-W. Zhang and Z.-T. Li, 2:2 Complexes from Diphenylpyridiniums and Cucurbit[8]uril: Encapsulation-Promoted Dimerization of Electrostatically Repulsing Pyridiniums, *Chem. - Asian J.*, 2018, **13**, 1312–1317.
48 M. Olesińska, G. Wu, S. Gómez-Coca, D. Antón-García, I. Szabó, E. Rosta and O. A. Scherman, Modular supramolecular dimerization of optically tunable extended aryl viologens, *Chem. Sci.*, 2019, **10**, 8806–8811.
49 H. Liu, Q. Pan, C. Wu, J. Sun, T. Zhuang, T. Liang, X. Mu, X. Zhou, Z. Li and Y. Zhao, Construction of two-dimensional supramolecular nanostructure with aggregation-induced emission effect via host–guest interactions, *Mater. Chem. Front.*, 2019, **3**, 1532–1537.
50 Y. Li, Y. Dong, X. Miao, Y. Ren, B. Zhang, P. Wang, Y. Yu, B. Li, L. Isaacs and L. Cao, Shape-Controllable and Fluorescent Supramolecular Organic Frameworks Through Aqueous Host–Guest Complexation, *Angew. Chem., Int. Ed.*, 2018, **57**, 729–733.
51 S.-Y. Jiang and X. Zhao, Soluble Two-dimensional Supramolecular Organic Frameworks (SOFs): An Emerging Class of 2D Supramolecular Polymers with Internal Long-range Orders, *Chin. J. Polym. Sci.*, 2019, **37**, 1–10.
52 Y. Zhang, T.-G. Zhan, T.-Y. Zhou, Q.-Y. Qi, X.-N. Xu and X. Zhao, Fluorescence enhancement through the formation of a single-layer two-dimensional supramolecular organic framework and its application in highly selective recognition of picric acid, *Chem. Commun.*, 2016, **52**, 7588–7591.
53 J. L. Belmonte-Vázquez, Y. A. Amador-Sánchez, L. A. Rodríguez-Cortés and B. Rodríguez-Molina, Dual-State Emission (DSE) in Organic Fluorophores: Design and Applications, *Chem. Mater.*, 2021, **33**, 7160–7184.
54 G. Xia, L. Si and H. Wang, Dual-state emission: the compatible art of substantial rigidity and twisting conformation within a single molecule, *Mater. Today Chem.*, 2023, **30**, 101596.
55 G. Chen, W. Li, T. Zhou, Q. Peng, D. Zhai, H. Li, W. Z. Yuan, Y. Zhang and B. Z. Tang, Conjugation-Induced Rigidity in Twisting Molecules: Filling the Gap Between Aggregation-Caused Quenching and Aggregation-Induced Emission, *Adv. Mater.*, 2015, **27**, 4496–4501.
56 G. Wu, Z. Huang and O. A. Scherman, Quantitative Supramolecular Heterodimerization for Efficient Energy Transfer, *Angew. Chem., Int. Ed.*, 2020, **59**, 15963–15967.
57 S. He, X. Sun and H. Zhang, Influence of the protonation state on the binding mode of methyl orange with cucurbiturils, *J. Mol. Struct.*, 2016, **1107**, 182–188.
58 Y. Tu, Z. Zhao, J. W. Y. Lam and B. Z. Tang, Mechanistic connotations of restriction of intramolecular motions (RIM), *Natl. Sci. Rev.*, 2021, **8**, nwaa260.
59 Z.-Y. Zhang and Y. Liu, Ultralong room-temperature phosphorescence of a solid-state supramolecule between phenylmethylpyridinium and cucurbit[6]uril, *Chem. Sci.*, 2019, **10**, 7773–7778.
60 Z.-Y. Zhang, Y. Chen and Y. Liu, Efficient Room-Temperature Phosphorescence of a Solid-State Supramolecule Enhanced by Cucurbit[6]uril, *Angew. Chem., Int. Ed.*, 2019, **58**, 6028–6032.
61 M. K. Kuimova, G. Yahioglu, J. A. Levitt and K. Suhling, Molecular Rotor Measures Viscosity of Live Cells via Fluorescence Lifetime Imaging, *J. Am. Chem. Soc.*, 2008, **130**, 6672–6673.
62 B. Pigulski, K. Shoyama, M.-J. Sun and F. Würthner, Fluorescence Enhancement by Supramolecular Sequestration of a C54-Nanographene Trisimide by Hexabenzocoronene, *J. Am. Chem. Soc.*, 2022, **144**, 5718–5722.
63 A. Pigliucci, G. Duvanel, L. M. L. Daku and E. Vauthey, Investigation of the Influence of Solute−Solvent Interactions on the Vibrational Energy Relaxation Dynamics of Large Molecules in Liquids, *J. Phys. Chem. A*, 2007, **111**, 6135–6145.